

# On the observability of spiral structures in CV accretion discs

D. Steeghs<sup>1</sup>, R. Stehle<sup>2</sup>

<sup>1</sup>*Physics and Astronomy, University of St. Andrews, North Haugh, St. Andrews, KY16 9SS, U.K.*

<sup>2</sup>*University of Leicester, Astronomy Group, Leicester LE1 7RH, U.K.*

Accepted 24 Feb 1999

## ABSTRACT

We use the grid of hydrodynamic accretion disc calculations of Stehle (1999) to construct orbital phase dependent emission line profiles of thin discs carrying spiral density waves. The observational signatures of spiral waves are explored to establish the feasibility of detecting spiral waves in cataclysmic variable discs using prominent emission lines in the visible range of the spectrum. For high Mach number accretion discs ( $M = v_\phi/c_s \simeq 15 - 30$ ), we find that the spiral shock arms are so tightly wound that they leave few obvious fingerprints in the emission lines. Only a minor variation of the double peak separation in the line profile at a level of  $\sim 8\%$  is produced. For accretion discs in outburst ( $M \simeq 5 - 20$ ) however, the lines are dominated by the emission from an  $m=2$  spiral pattern in the disc. We show that reliable Doppler tomograms of spiral shock patterns can be reconstructed provided that a signal to noise of at least 15, a wavelength resolution of  $\sim 80 \text{ km s}^{-1}$  and a time resolution of  $\sim 50$  spectra per binary orbit is achieved. We confirm that the observed spiral pattern in the disc of IP Pegasi can be reproduced by tidal density waves in the accretion disc and demands the presence of a large, hot disc, at least in the early outburst stages.

**Key words:** accretion, accretion discs – shock waves – novae, cataclysmic variables — binaries: close

## 1 INTRODUCTION

Cataclysmic variables (CVs) harbour a geometrically thin viscous accretion disc through which mass from a late type companion star is accreted onto a white dwarf. Rapid brightness variations of several magnitudes displayed by the sub class of dwarf novae indicate that information is transported along the accretion disc on a viscous time scale of a few days (see Warner 1995 for an extensive review). The dynamical time scale of disc material on the other hand, is given by the local Kepler velocity and ranges from seconds near the white dwarf, to a considerable fraction of the orbital period (hours) at the outer disc. The effective viscous transport displayed by these discs demands the presence of a highly efficient source of angular momentum transport within the discs, whose physical origin is poorly understood.

The convenient time scales in CVs allow us to study the changing properties of viscous accretion discs in real-time. As the accretion disc is viewed from different angles during a binary orbit, image reconstruction techniques (IRTs) such as eclipse mapping (Horne 1985) or Doppler tomography (Marsh & Horne 1988) are able to provide spatially resolved images of accretion discs on a micro-arcsecond scale. Since

IRTs use the luminosity variation of the disc with binary phase during a considerable fraction of the binary orbit, the reconstructed images are time averaged pictures of the disc pattern. This implies that IRTs can reconstruct those disc features which are stable over a period comparable to a dynamical time scale in the co-rotating frame of the binary.

Numerical calculations by various authors (e.g. Sawada, Matsuda & Hachisu 1986, Różycka & Spruit 1993, Heemskerk 1994, Larwood 1997, Yukawa, Boffin & Matsuda 1997, Stehle 1999) show that tidally induced waves can result in two prominent spiral shock arms, which are stationary on a dynamical time scale in a co-rotating frame. The shocks are excited in the outer disc by the tidal action of the secondary star. In the binary potential field, the disc gas revolves around the white dwarf on non-axisymmetric orbits where the streamline–density for a pressure free gas is highest towards the secondary and lowest normal to it (Paczyński 1977). In a low–temperature disc, the shape of the streamlines are still similar to the pressure free gas, but the variation of the streamline–density with azimuth along a particle orbit will excite pressure waves which steepen to shock waves while they travel inward (Spruit, Matsuda, Inoue & Sawada 1987). Additionally, shocks can be excited by

arXiv:astro-ph/9902358v1 25 Feb 1999

the crossing of particle orbits if the disc is larger than the tidal radius. The opening angle of the shock arms depend mainly on the azimuthal Mach number  $M = v_\phi/c_s$  with  $v_\phi$  the azimuthal disc gas velocity and  $c_s$  the sound speed, i.e. on the rate with which the shock is sheared by differential rotation of the disc gas while the shock travels inward radially (Różyczka & Spruit 1989).

A strong radial viscous force, if present in accretion discs, may on the other hand damp the shocks over a short range or may even prevent the pressure disturbance to steep into a shock firsthand (Savonije, Papaloizou & Lin 1994). As the origin of the viscosity is not known, we neglect in our calculations any radial viscous forces and thus derive a maximum amplitude for the shocks. If this is a sensible assumption is one of the main questions to be answered by comparing accretion disc models with yet to come detailed observations.

Despite the firm prediction of shocks in accretion discs, two armed spiral signatures have only recently been found by Steeghs, Harlaftis & Horne (1997) and Harlaftis et al. (1999) in the eclipsing CV IP Pegasi during outburst. Doppler tomograms revealed a strong two-armed spiral pattern in the outer disc. Even though Doppler tomography is ideally suited to detect asymmetric disc structures (see e.g. Robinson, Marsh & Smak 1993), it is unclear if previous observations failed in reconstructing spiral arms because of insufficient data quality or because spiral arms were not present in the disc at the time of the observation. To clarify this question the purpose of this paper is to predict observational signatures of tidal density waves in high  $M$  and low  $M$  accretion discs, the latter appropriate for accretion discs during dwarf nova outbursts.

We use the emission line model of Horne (1995) to calculate emission line profiles for various binary configurations, using the grid of full hydrodynamic disc calculations by Stehle (1999) as underlying models.

The paper is organized as follows: in Section 2 we will introduce our time averaged model calculations and our method of constructing Doppler tomograms and line profiles. In Section 3 we present model predictions for several relevant cases. The effect of instrumental resolution and signal to noise on the detectability of tidal structure is explored in Section 4. We conclude the paper in Section 5 with a discussion and summarize our results in Section 6.

## 2 EMISSION LINES FROM SPIRAL SHOCKS

### 2.1 The grid of hydrodynamic disc models

As our underlying disc models we use the grid of geometrically thin 2D-disc calculations by Stehle (1999). The disc thickness is explicitly followed by two additional equations in a one-zone model (see Stehle & Spruit 1999 for a detailed description). The spatial and temporal evolution of the disc temperature follows tidal and viscous heating, the latter in the  $\alpha$ -ansatz of Shakura & Sunyaev (1973), as well as radiation from the disc surfaces.

Our time dependent calculations were time averaged over at least one binary orbit in the co-rotating frame of the binary, i.e.

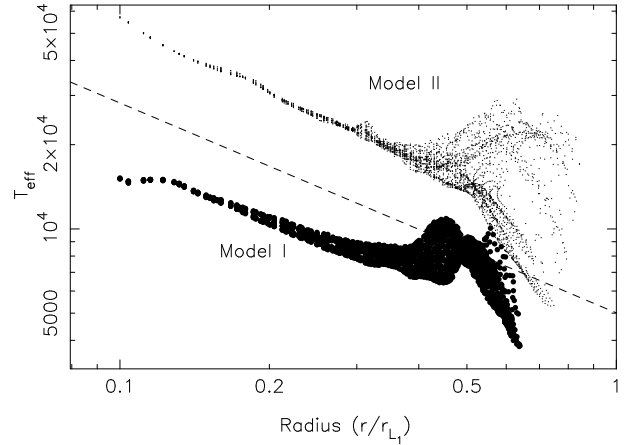


**Figure 1.** The effective temperature  $T_{\text{eff}}(r)$  versus the disc radius  $r/r_{L1}$  for models I ( $\alpha = 0.01$ , lower line) and II ( $\alpha = 0.3$ , top line).  $T_{\text{eff}}(r)$  follows closely the power  $r^{-3/4}$  (dashed line), as expected for hot, stationary accretion discs. Near the outer disc edge, the effects of tidal heating and non-axisymmetry result in a wide range of disc temperatures.

$$\bar{f} = \frac{1}{t_f - t_i} \int_{t_i}^{t_f} f(t) dt \quad (1)$$

where  $f$  is any conservative physical quantity, like the momentum in radial direction  $p_r$ , the angular momentum  $p_\phi$ , the vertical momentum  $p_z$ , the surface density  $\Sigma$  or the internal energy density  $e$ . Other quantities, as e.g. the disc gas velocity, are derived from the time averaged values. We will deal further on only with time averaged values and thus we subsequently drop the bar in our notation for convenience. By averaging our models in time, only those disc features which are reasonably stable over a dynamical time scale will still be visible.

We will be presenting the results of two model simulations. Both models are simulations of the accretion disc in a binary with mass ratio  $q = M_2/M_1 = 0.3$  and orbital period  $P = 2.3$  hours. The  $\alpha$ -type Shakura & Sunyaev viscosity in model I is 0.01 and we time-averaged over  $\sim 1.5$  binary orbits. Model II represents a typical dwarf nova outburst disc with  $\alpha = 0.3$ , time averaged over  $\sim$  one orbital period. We also calculated model predictions for various other mass ratios and different averaging times which all share the same qualitative features since the spiral arms are very stable in the binary frame and mainly depend on the disc temperature (see also Stehle 1999). These two models in particular were selected as a typical comparison between a small, cool disc (I) versus a large, hot viscous disc (II) illustrative for the discs in CVs. We show in Fig. 1 the run of  $T_{\text{eff}}$  with disc radius  $r$  in units of the distance to the  $L_1$  point. In both cases  $T_{\text{eff}}(r) \propto r^{-3/4}$  in the inner parts of the disc, as expected from stationary viscous accretion discs. Close to the outer disc edge though, tidal heating and non-axisymmetry result in the large spread of  $T_{\text{eff}}(r)$ .

### 2.2 Doppler tomograms and line profiles

For our analysis we use a right-handed Cartesian coordinate system  $(\vec{e}_x, \vec{e}_y, \vec{e}_z)$  centred on the white dwarf, with the positive X-axis in the direction of the secondary star and

$\vec{e}_z$  parallel to the rotation vector of the accretion disc. The disc gas velocities are transferred to inertial velocities corresponding to the centre of mass of the binary. To calculate the line emissivity for each disc grid cell, we follow the lines of Horne & Marsh (1986) and Horne (1995). The emission line surface brightness  $J$  is obtained by integrating over the local line profile times the foreshortening due to the orbital inclination  $i$ ;

$$J = \cos i \int S_L (1 - \exp(-\tau_\nu)) d\nu \quad (2)$$

In the case of optical thin line emission,  $J(x, y)$  is proportional to the surface density  $\Sigma(x, y)$  and the local line source function  $S_L(\lambda)$ . However, most strong emission lines such as the hydrogen Balmer series are optically thick and saturated. The area under the profile is then well approximated by the product of  $S_L$  and the frequency interval over which the optical depth exceeds unity. Using eq. (15) from Horne (1995), the local line emissivity of a saturated emission line with rest wavelength  $\lambda_0$  is in that case given by:

$$J(x, y) = S_L \frac{\Delta V}{\lambda_0} \cos i \sqrt{8 \ln \tau_0} \quad (3)$$

$\Delta V$  is the total velocity dispersion along the line of sight,  $\tau_0$  the optical depth of the centre of the emission line. If we furthermore assume local thermodynamic equilibrium,  $S_L$  equals the Planck function. The velocity dispersion consists of a thermal component  $V_{\text{th}} = \sqrt{kT/m_H A}$ , with  $m_H$  the mass of a hydrogen atom and  $A$  the atomic weight, and a shear term  $V_{\text{shear}}$ , derived from the full, non-Keplerian, velocity field.  $\Delta V$  is evaluated for each grid cell and viewing angle according to

$$\Delta V^2 = V_{\text{th}}^2 + V_{\text{shear}}^2 \quad (4)$$

where

$$V_{\text{shear}} = \frac{\Delta Z}{\cos i} \vec{e} \cdot \vec{\nabla} \vec{V} \cdot \vec{e} \quad (5)$$

$$= \frac{\Delta Z}{\cos i} \vec{e} \cdot \begin{pmatrix} \frac{\partial V_x}{\partial x} & \frac{\partial V_y}{\partial x} & \frac{\partial V_z}{\partial x} \\ \frac{\partial V_x}{\partial y} & \frac{\partial V_y}{\partial y} & \frac{\partial V_z}{\partial y} \\ \frac{\partial V_x}{\partial z} & \frac{\partial V_y}{\partial z} & \frac{\partial V_z}{\partial z} \end{pmatrix} \cdot \vec{e} \quad (6)$$

$\vec{e}$  denotes the earth vector pointing from the grid cell towards the observer, and  $\vec{\nabla} \vec{V}$  is the tensor of the local velocity gradient including all anisotropic terms. In this way the velocity field of our simulations self consistently provides the total velocity dispersion along each line of sight.  $\Delta Z$  denotes the vertical extent of the emission line layer and is assumed to be  $0 \leq \Delta Z \leq H$ .

Since  $\tau_0 \propto \Sigma/\Delta V$  we derive:

$$J(x, y, \phi, i) \propto B_\nu(T_{\text{eff}}) \Delta V(x, y, \phi, i) \sqrt{\ln\left(\frac{\Sigma(x, y)}{\Delta V(x, y, \phi, i)}\right)} \quad (7)$$

The line emissivity is mainly sensitive to the local velocity dispersion  $\Delta V$ . The large gradients across the spiral shocks will therefore enhance the local emissivity of saturated lines significantly at the location of the spiral arms.

The line emissivity is transformed from position  $(x, y)$  to velocity coordinates  $(V_x, V_y)$  by multiplying with the Jacobian of the coordinate transformation, i.e.

$$J(V_x, V_y) = \left| \begin{array}{cc} \frac{\partial V_x}{\partial x} & \frac{\partial V_x}{\partial y} \\ \frac{\partial V_y}{\partial x} & \frac{\partial V_y}{\partial y} \end{array} \right|^{-1} J(x, y). \quad (8)$$

For each binary phase  $\phi$  the line profile  $f(v, \phi)$  is synthesised by adding up the individual contributions of the grid cells where the emission line contribution is Doppler shifted according to the local gas velocity along the line of sight,  $V_{\text{dop}} = -\vec{V} \cdot \vec{e}$ . We adopt the usual convention that phase 0.0 corresponds to inferior conjunction of the companion star, i.e. mid-eclipse in high inclination systems. The visibility of each grid cell is tested for eclipses by the companion star which we assume to fill its critical Roche volume. Self-shadowing of the disc, important for high-inclination CVs due to the vertically extended disc rim will be discussed elsewhere (Stehle & Steeghs, MNRAS, in preparation).

The above description to construct emission line profiles holds principally for all *saturated* emission lines. We choose the Hydrogen  $\beta$  line at 4861Å as our reference line for most calculations. The Balmer lines are the most prominent lines in CV spectra and allow disc reconstructions at a high signal to noise. It serves as a typical representative line observed in optical emission line studies of CVs. Since we are concerned with the dynamical properties of the line profiles rather than calculating absolute line strengths, this particular choice does not affect our subsequent analysis. To illustrate the effects of saturation we will calculate both the case of no shear and maximum shear broadening as well as compare with the properties of a heavy element such as Calcium.

### 3 MODEL PREDICTIONS

In this section we present predicted emission line profiles and Doppler tomograms for the disc models limited only by the finite grid resolution of our hydrodynamical calculations. As we will see in Sec. 4, the limits set by the instrumentation will dominate over our limited numerical grid resolution and it is thus appropriate to call our tomograms in this Section “ideal”. We identify the signatures of spiral waves in the emission lines of accretion discs. As the global shape of the spiral shocks is characterised by the Mach number of the disc, we present our model predictions in descending order of  $M$ .

#### 3.1 Axisymmetric discs

The properties of emission lines from axisymmetric accretion discs have been investigated by several authors (e.g. Smak 1981, Horne & Marsh 1986), of which we summarise a few relevant features. The large Kepler velocities of a few thousand  $\text{km s}^{-1}$  in the inner disc down to several hundreds  $\text{km s}^{-1}$  in the outer disc, produce very broad emission line profiles, decoupling the global shape of the line from the local line radiative transfer. A double peak shape results where the peak velocities reflect the motion of the gas at the outer disc edge, which in turn can be used to estimate the size of the disc if a velocity field, such as Keplerian, is assumed.

The orbital velocity of the white dwarf is sometimes estimated by measuring the centroid of the observed line profile, which should show a sinusoidal dependence with orbital phase as the white dwarf orbits around the binary center of mass. While the line profile as a whole thus moves, the separation between the double peaks is constant with

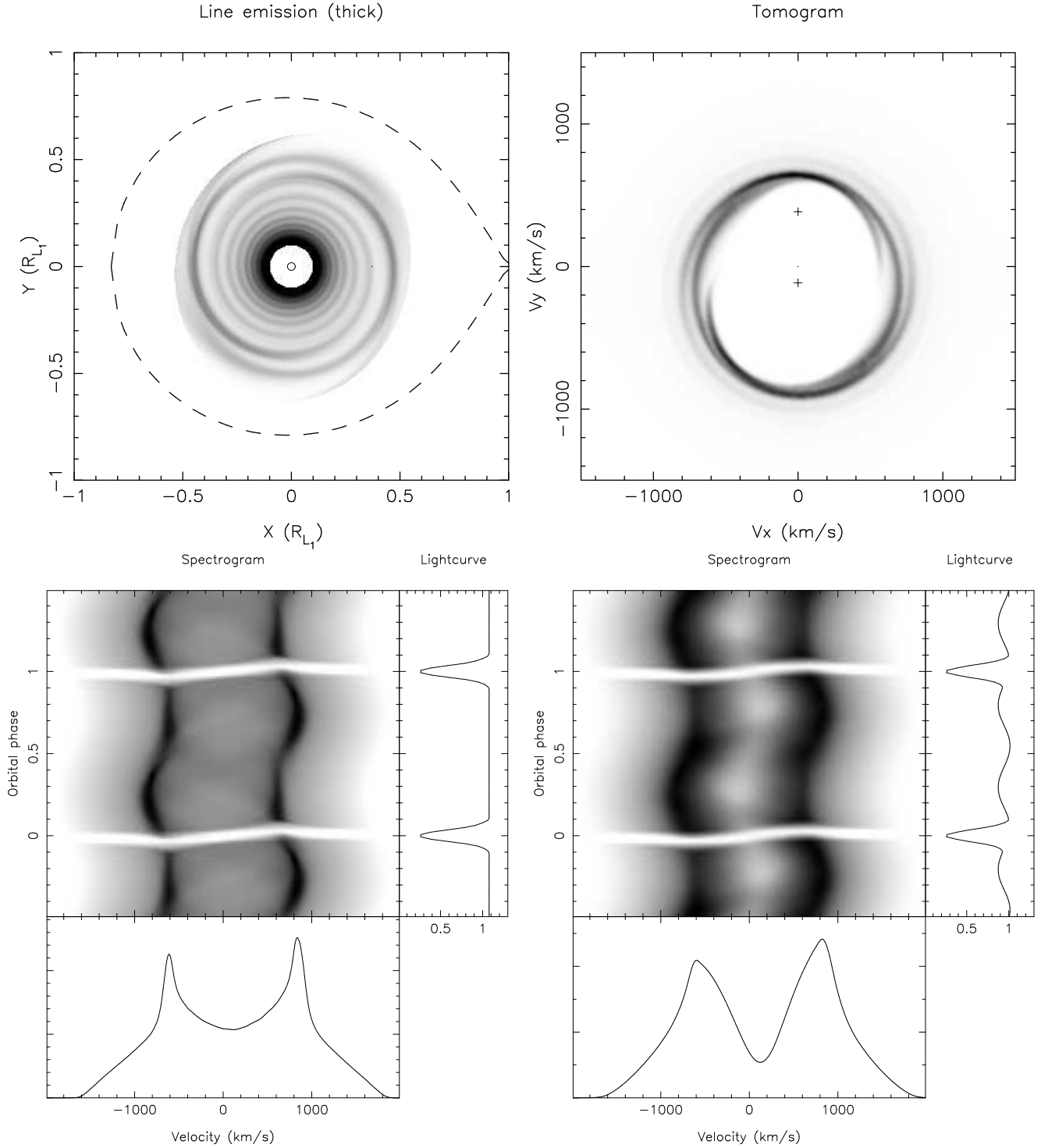


**Figure 2.** Model I: an  $\alpha = 0.01$  disc in a binary with  $q = M_2/M_1 = 0.3$ . Top panels show the distribution of line emission in both spatial coordinates (left) as well as in the  $V_x V_y$ -plane. The crosses in the tomogram denote the projected radial velocity of the white dwarf (lower cross) and secondary star. Bottom panels display the calculated emission line profiles for Hydrogen-like lines at an inclination of  $80^\circ$ . Bottom left with no shear broadening (i.e. a thin emission line layer), right with maximum shear broadening when line emission is produced across the whole disc height. To the right of each trailed spectrogram is the total line flux light curve, and below it the emission line profile at orbital phase 0.75.

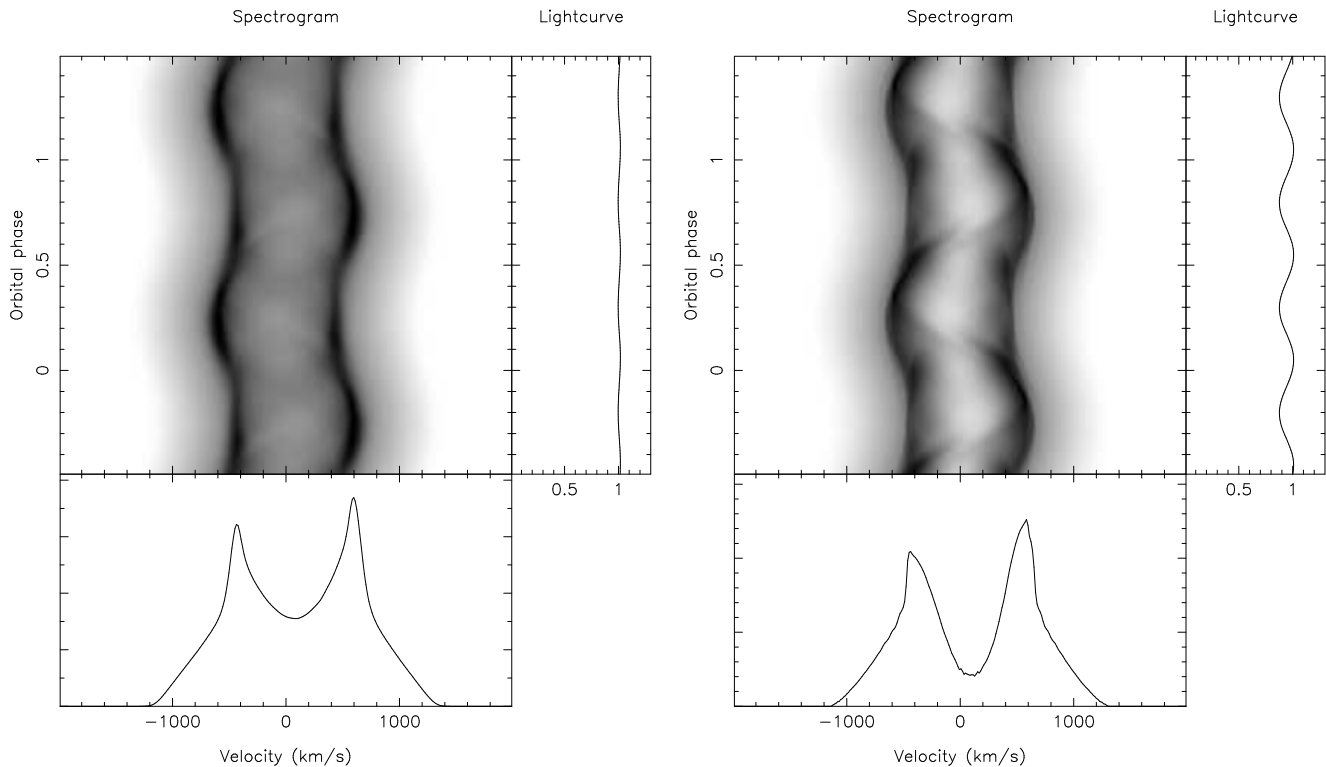


**Figure 3.** The effect of atomic weight on the shear broadened profiles. Left are the line profiles for Model I viewed at an inclination of  $i = 45^\circ$  for a Hydrogen line ( $A=1$ ). Right panel is for a saturated Calcium line ( $A=40$ ). Because of the much smaller thermal velocity in the case of Calcium, the shear broadening is much stronger than for Hydrogen lines. This results in a stronger signature of spiral waves in the emission lines.

phase. In the velocity coordinate space of Doppler tomograms, axisymmetric discs will produce axisymmetric circular images, centered on the radial velocity of the white dwarf ( $V_x = 0, V_y = -K_1$ , with  $K_1$  the projected orbital velocity of the white dwarf). For each radius, a corresponding ring at the local disc velocity is produced, with the smallest velocities corresponding to the outer edge.

### 3.2 Model I: High Mach number disc

In Fig. 2 we show the model predictions for the high Mach number CV disc of model I, viewed at an inclination of  $80^\circ$ . The spatial distribution of the line emission is plotted in the top left panel and displays a rather small disc, varying in radius between  $r_{\text{out}}(\phi) \simeq 0.55 - 0.65 r_{L1}$ , with two tightly wound spiral shock arms covering the disc down to small radii. If we plot the same distribution in velocity coordinates (top right), the typical ring shape appears, with the two shock arms visible as sharp arcs of enhanced line emissivity in the top and bottom areas. The outer disc edge provides a cut off of any emission with velocities lower than  $\sim 600 \text{ km s}^{-1}$  while at high velocities, the inner disc, the tomogram becomes more symmetrical. The emission line profiles in the corresponding trailed spectrograms (Fig. 2, bottom panels) feature two sharp peaks, reflecting the velocities of the outer disc gas. Two cases are plotted to illustrate the effect of shear broadening due to the finite thickness of the emission line region (Horne & Marsh 1986). In the bottom left panels, the emission line layer is assumed to be very thin ( $\Delta Z/H \simeq 0$ ), so that shear broadening effects vanish and sharp and

narrow double peaks are formed. This is very similar to the optical thin case. On the right is the case of maximum shear broadening, assuming the emission lines are formed across the full disc thickness such that  $\Delta Z = H$  in eq. (5). Broad peaks with a V-shaped, rather than U-shaped valley between the peaks are formed.

The presence of spiral arms slightly distorts the velocity of the peaks as a function of binary phase, varying between  $v_{\text{peak}}(\phi) = 690 - 750 \text{ km s}^{-1}$  with respect to the white dwarf. On average, the double peak separation is  $\langle v_{\text{peak}} \rangle = 725 \text{ km s}^{-1}$ . This corresponds to a disc radius of  $r_{\text{out}} \simeq GM_1/(v_{\text{peak}})^2 = 0.61 r_{L1}$ , assuming Keplerian velocities. While the disc is slightly tidally distorted and elongated along the Y-direction, the assumption of Keplerian velocities still provides a reliable estimate of the average disc size in this case.

Shear broadening can be particularly important for heavy elements. Their low thermal velocity results in a stronger local enhancement of the line flux due to velocity gradients. To illustrate this, Figure 3 shows the line profiles of a light element ( $A=1$ ) versus that of Calcium ( $A=40$ ) at an inclination of  $45^\circ$ . While for hydrogen like lines the shear broadening is no longer important due to foreshortening, the Calcium line displays strong anisotropic components originating along the spiral arms. This increases the double peak variation from 8% in the case of no shear to 13% for maximal shear in heavy lines such as Calcium.

The orbital variation in the separation of the double peaks, is the predominant signature that the disc is asymmetric and that the emissivity is not uniform. In the case

of considerable shear broadening, the line emission from the spiral shocks is additionally non-isotropic resulting in a binary phase dependent variation of the peak strengths with a maximum at phases 0.25 and 0.75 as is visible in the emission line flux light curves to the right of the spectrograms. Such non-isotropic line emission cannot be modelled by Doppler tomography, since only the average line flux at a given velocity is provided, but can be identified in the emission line profiles directly as a signature of shocks in the outer disc. While saturated emission lines from heavy elements are thus good indicators of large velocity gradients, they are unfortunately usually weak lines and do not provide sufficient signal to noise for Doppler imaging in existing data sets.

### 3.3 Model II: dwarf nova outbursts

By increasing the parameter of the small scale viscosity to  $\alpha = 0.3$  in Model II, viscous spreading becomes more efficient in pushing the accretion disc towards larger radii of  $r_{\text{out}}(\phi) \simeq 0.6 - 0.8 r_{\text{L1}}$  (see Fig. 4, top left panel). The increased local viscous heating additionally produces higher disc temperatures, and thus lower Mach numbers, now of the order  $M \sim 5 - 20$ . This is reflected in the open geometry of the two spiral shock arms in the outer disc. In Fig. 4 we present the calculated emission line properties for model II, again at an inclination of  $i = 80^\circ$ .

It is difficult to assign a meaningful disc radius as the line emissivity is predominantly localized at the two spiral arms. The strong  $m=2$  spiral wave pattern in the outer disc dominates the corresponding Doppler tomograms, shown in the top right panel of Fig. 4. The line emission extends towards lower velocities ( $\sim 500 \text{ km s}^{-1}$ ), partly because of the increased disc size, and partly because sub-Keplerian motions are significant in these outer regions. Figure 5 shows the deviation from Keplerian velocities at a few representative radii. While the disc is close to Keplerian in its inner regions (high velocities), the departures at the outer disc near  $v \sim 500 \text{ km s}^{-1}$  are significant and of the order of  $\sim 100 \text{ km s}^{-1}$ .

The line profiles are easily distinguishable from an axisymmetric disc. The  $m = 2$  spiral pattern results in converging emission line peaks, with a cross over near phases 0.25 and 0.75. This contrasts to the axisymmetric case, with a constant double peak separation, independent of orbital phase. Though a non-circular disc could also produce a variation in the double peak separation with phase, it would not produce the existence of multiple peaks as one crosses from one spiral arm to the next, with a corresponding sudden jump in velocity of several hundred  $\text{km s}^{-1}$ , a unique signature of a spiral shock pattern. Again the large velocity gradients are important at high inclinations where shear broadening can dominate. This produces a variation in the emission line light curve (Fig. 4 bottom right panel) which is considerably larger compared to Model I.

## 4 RECONSTRUCTING SPIRAL STRUCTURES IN CV DISCS

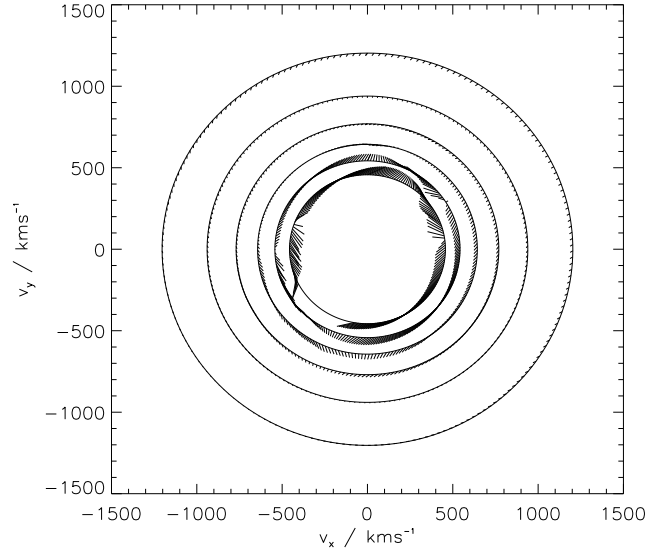


**Figure 5.** Non-Keplerian velocities in model II. The circles denote the Kepler velocity at a few radii in the disc. The small ticks point to the actual disc velocity at that radius and azimuth. The tidal distortions become prominent in the outer disc, i.e. at low velocities in the inner regions of the Doppler maps.

### 4.1 Realistic data quality

In the previous section we discussed our model predictions limited by the grid resolution of our hydrodynamical models. We now include instrumental noise and finite spectral/time resolution in our predicted data to provide a realistic comparison with observed data and constrain the necessary data requirements to reconstruct tidal arms in CV discs.

Three instrumental effects play a role. First the wavelength resolution of the individual spectra, setting a limit to the velocities that can be resolved. The emission lines typically span several thousands of  $\text{km s}^{-1}$ , which need to be sampled by ample number of pixels. On the other hand, resolutions much better than the width of the local line profile ( $\sim 10 \text{ km s}^{-1}$ ) are not providing any additional information. A resolution of  $\sim 20-80 \text{ km s}^{-1}$  is therefore usually optimal, though is practically limited by signal to noise requirements.

Secondly, the phase or time resolution has to be short enough to provide sufficient phase sampling across the binary orbit to avoid artifacts in the image reconstruction (see also Marsh & Horne 1988). The higher the resolution of the input data, the more projections are required to provide sufficient sampling and exploit the available resolution. To avoid under sampling the image one typically needs at least 50 orbital phases.

Finally, the signal to noise of the individual spectra will determine how well the data will constrain the image structure. In the case of maximum entropy reconstruction as is the case here, the reconstructed image is a balance between fitting the data using maximum likelihood statistics and selecting the simplest image using the maximum entropy criterion.

To test the importance of above mentioned effects, we start by calculating ideal line profiles (such as presented in Section 3) for an inclination of  $45^\circ$  at 50 orbital phases equally spaced over the binary orbit. The data is then convolved with a Gaussian with FWHM equal to the desired

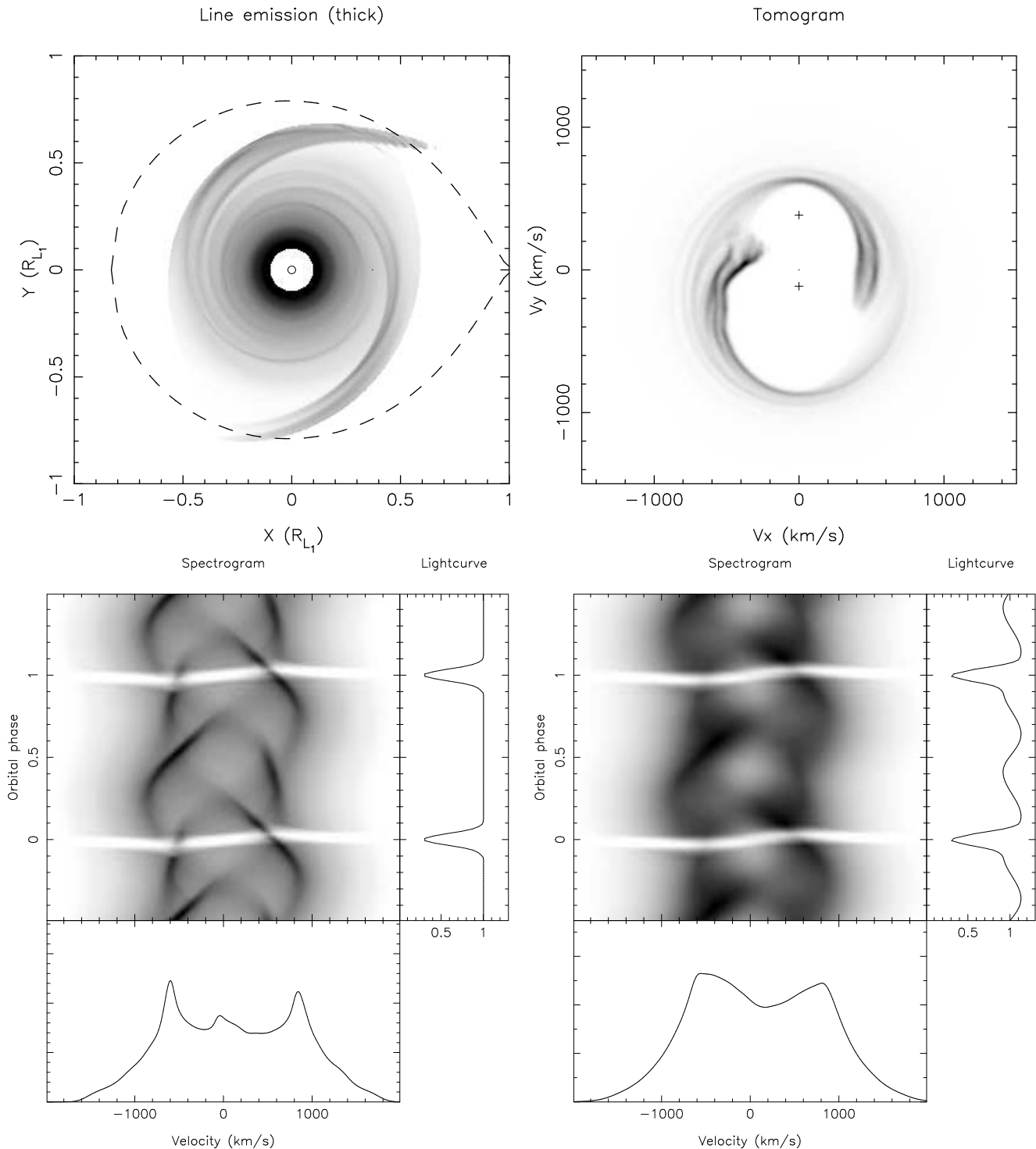


**Figure 4.** As Fig. 2 but now for the low Mach number disc of model II.

instrumental resolution and binned in wavelength such that 2 data pixels cover the instrumental profile. Poisson noise was subsequently introduced to achieve different signal to noise levels in the line profiles as follows. We added a continuum to our line profiles such that the line strength (line - continuum) equals about two times the continuum level, a typical value for the strong emission lines in dwarf novae. Poisson noise was then added to achieve the desired signal

to noise level in the continuum. Using the synthetic noisy data, we construct maximum entropy Doppler tomograms using the same code that is used for the observations \*

\* DOPPLER package developed by Tom Marsh, see <http://www.astro.soton.ac.uk/~trm/software.html>

## Model I

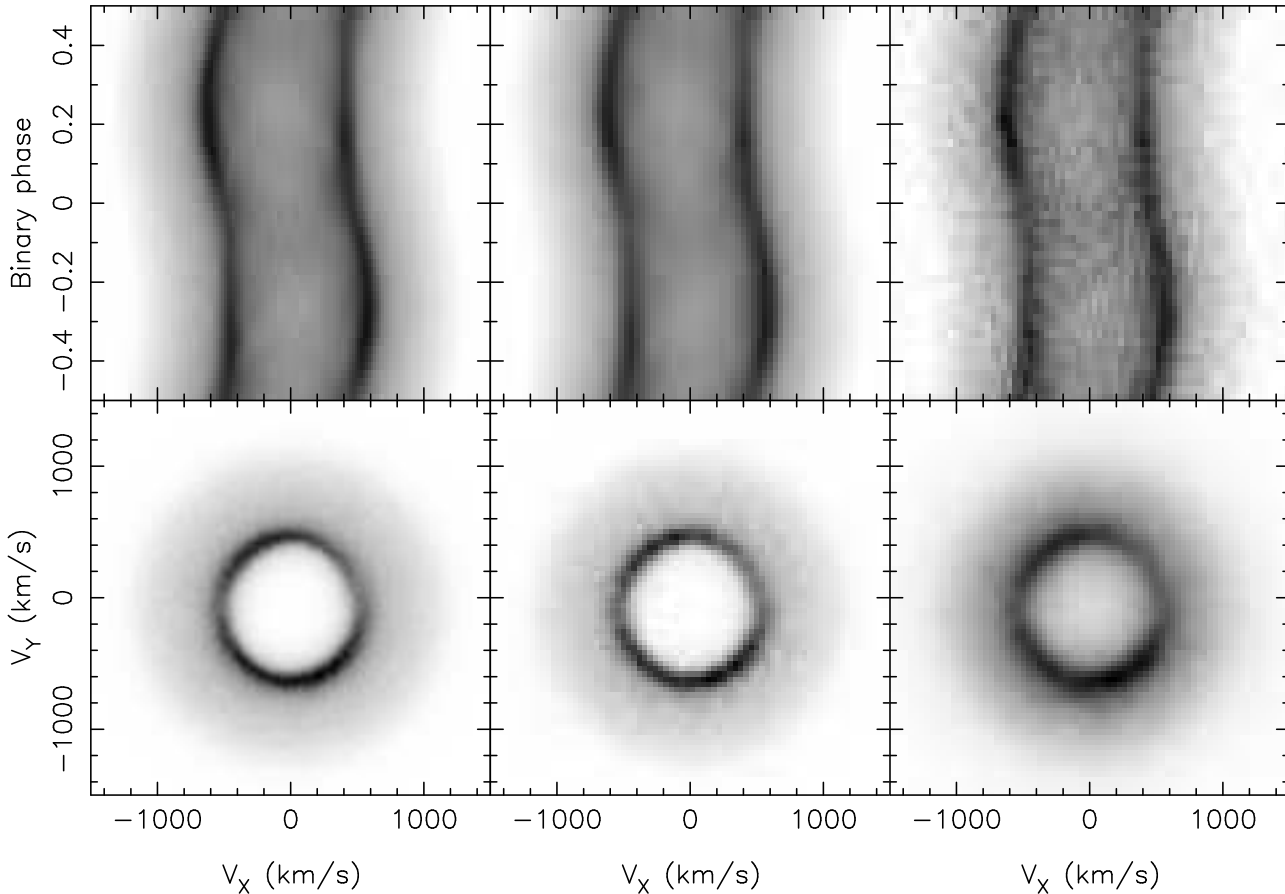


**Figure 6.** Tomograms and trailing spectra of the high Mach number simulation (model I) for a strong emission line. From left to right the 2-pixel wavelength/velocity resolution is (40, 80, 80)  $\text{km s}^{-1}$  and the ratio of signal to noise is (50, 50, 15) in the continuum.

#### 4.2 High M model

Figure 6 shows the image reconstructions based on model I, at an inclination of  $45^\circ$  and including maximum shear broadening. The top panels show the simulated data, the left has a 2-pixel resolution of  $40 \text{ km s}^{-1}$ , the middle and right have a resolution of  $80 \text{ km s}^{-1}$ . The signal to noise in the left and middle panels is  $\sim 50$  in the assumed continuum, while for the right panel it is degraded to  $\sim 15$ . Below each spectrogram the reconstructed Doppler tomograms are shown, all on the same scale.

It is difficult to reconstruct a clear signature of the tightly wound spiral waves. Except for an enhancement of the disc emission in the top left and lower right, such discs will look very similar to axisymmetric discs, even if high quality data is available. As data quality is degraded the slight variation of the double peaks with binary phase becomes difficult to measure. We conclude that we do not expect to see obvious evidence of spiral waves in Doppler maps of small, low  $\alpha$  accretion discs even if tightly wound spiral waves are present.

#### 4.3 Low M model

Figure 7 plots similar reconstructions now based on model II. Resolution and signal to noise levels are identical to the previous model for comparison. The strong two armed spiral pattern is readily recovered even at low signal to noise and medium resolution (Fig. 7, right). In these large hot discs, the tidal arms dominate the emission lines and are easily visible both in the line profiles directly and in Doppler tomograms.

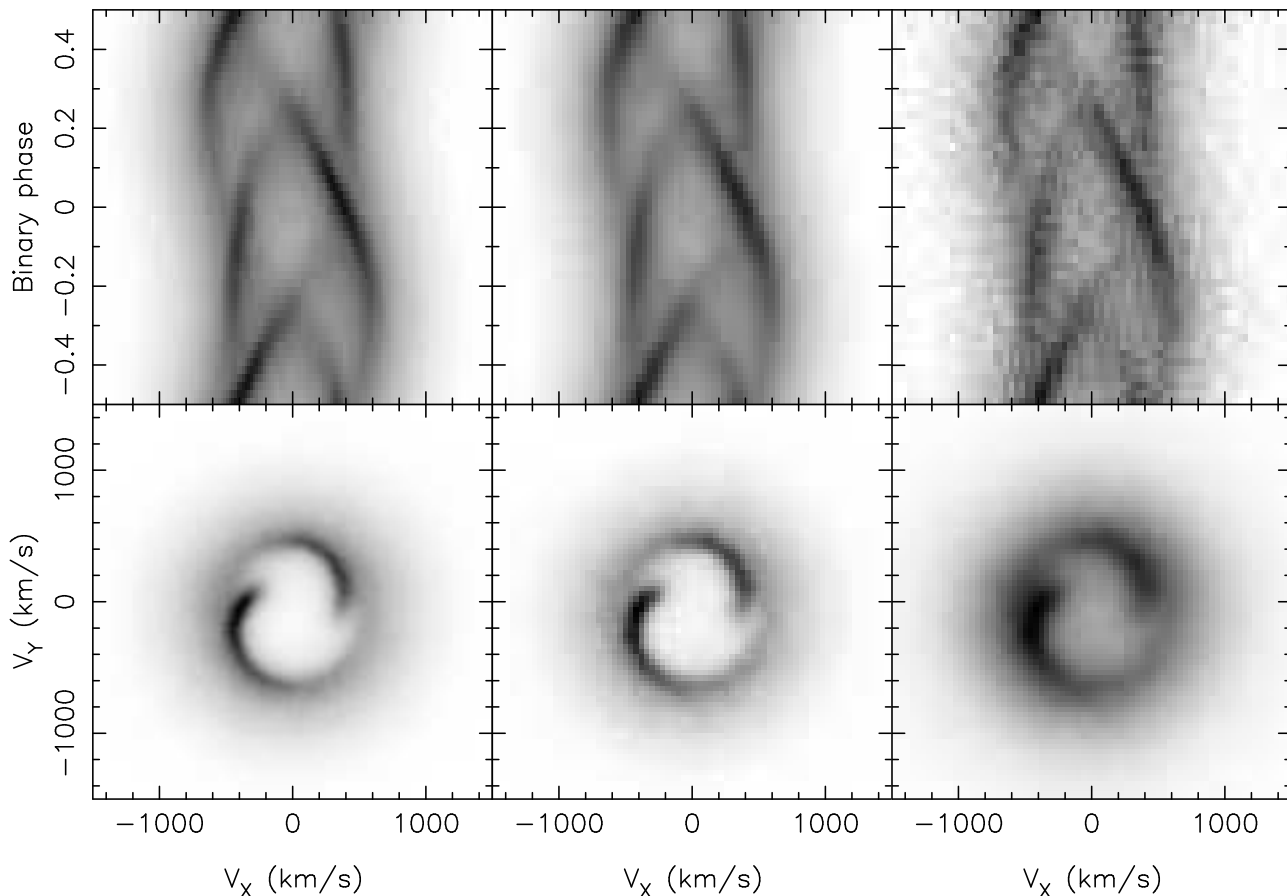
To compare the two models, we show the asymmetric part of the reconstructed tomograms in Fig. 8. These are obtained by subtracting the median of the image at each velocity, measured from the white dwarf. The low Mach number case (bottom) shows prominent spiral arms, whereas for model I, only a slight asymmetry is observed.

#### 4.4 Instrumental requirements

We reconstructed disc images for various signal to noise levels, amounts of shear broadening, orbital inclinations and number of binary phases using Model II data. Based on these reconstructions, we found a signal to noise of  $\sim 15$  in the line flux and a two pixel velocity resolution of  $\sim 80 \text{ km s}^{-1}$  to be sufficient to convincingly reproduce the two armed pattern



Model II

**Figure 7.** As Fig. 6 but for model II

on the disc. As we mentioned earlier, to avoid artifacts  $\sim 50$  orbital phases are desired. The instrumental requirements for reconstructing such open spirals are therefore fortunately relatively modest and suggest a search for such structure in CV discs is feasible and will provide strong constraints on the presence of spiral waves in these discs.

Figure 9 illustrates some of the reconstructions obtained. The left two images illustrate the effect of shear broadening for high inclination cases. The disc image is similarly broadened in the case of strong shear broadening but still carries the two armed pattern. Middle panels illustrate the effect of a strong versus weak emission line. This basically lowers the signal to noise of the data and affects the disc image in the same way. Finally the right panels show the strong artifacts due to poor phase sampling (top) or the lack of image structure due to poor resolution.

#### 4.5 Other emission line sources

Our reconstructed images are those of the accretion disc contribution only. The irradiated companion star, the gas stream and the hot spot are well known other contributors to the emission line flux. In the case of the companion star, its contribution is confined to a Roche lobe shape centered at the radial velocity of the companion, at velocities where no

disc emission is expected. More demanding are the stream-disc interactions, which can contribute to a wider range of velocities overlapping the accretion disc, though the compact impact region is usually well defined. Complicated are disc outflows, which can be responsible for the single peaked emission lines observed in some systems. These issues have to be born in mind when interpreting emission line data sets (e.g. Steeghs, Horne, Marsh & Donati 1996).

## 5 DISCUSSION

The Doppler images and line profiles presented in this paper, confirm that the observed disc structure in tomograms of IP Pegasi can be reproduced by tidally excited spiral arms in the disc. The presence of a dominating two armed structure in early outburst, when the disc is hot and large, compared to a fairly symmetric disc in quiescence matches extremely well with the model predictions presented here. Armitage & Murray (1998) reach a similar conclusion based on 3-D SPH simulations of the disc flow in IP Pegasi. A spiral density pattern, matching the kinematics of the observations, is formed when  $\alpha$  is increased and the disc expands. However, these arms appear to be transient in their simulations on a viscous time scale. In the models of Stehle (1999) the spiral

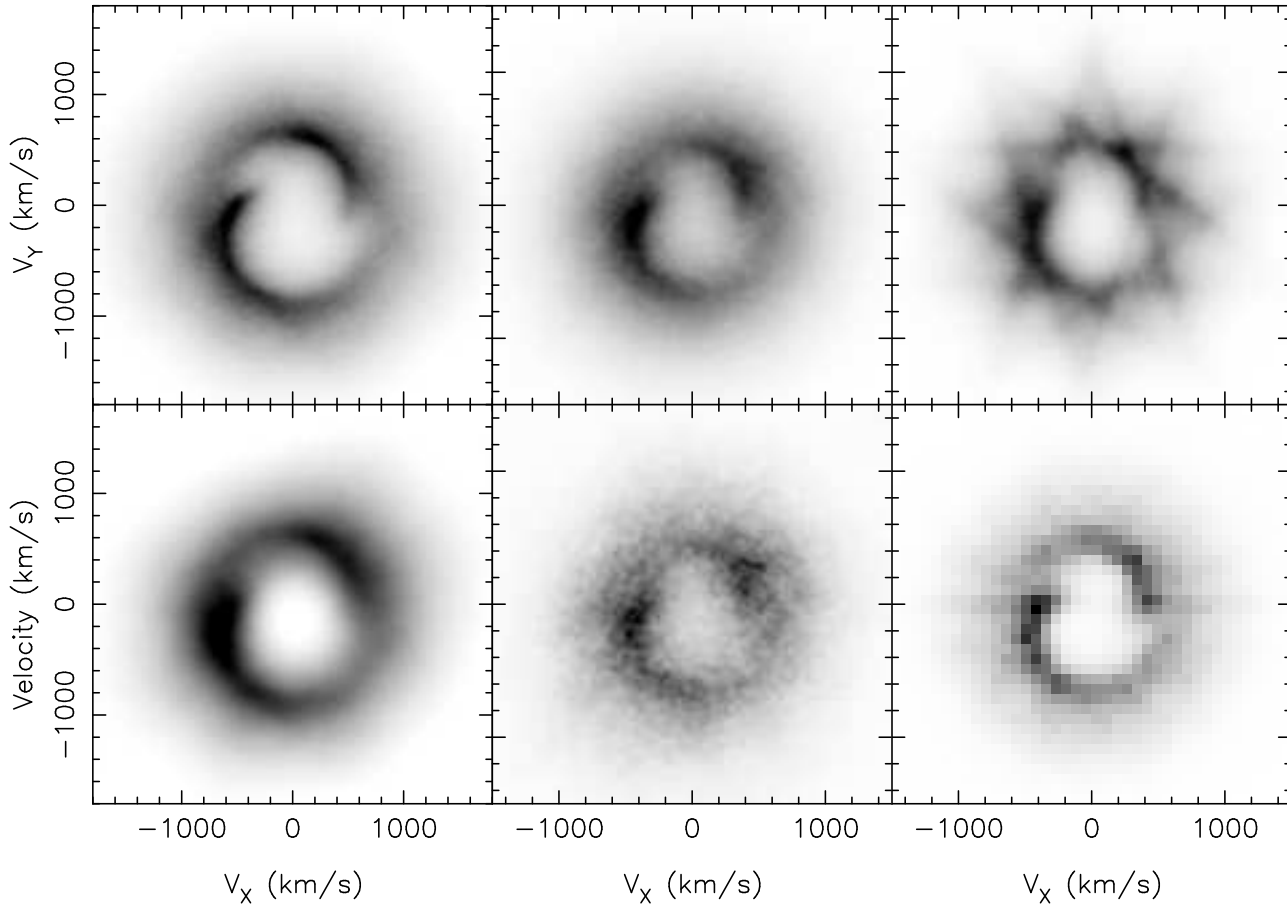


**Figure 9.** Some example reconstructions for Model II data. Left is the case of high inclination ( $80^\circ$ ) without (top) and with maximal shear broadening. Middle a reconstruction of a strong emission line (twice the continuum) with a continuum signal to noise of 30 (top) compared to a weak line (15% above continuum) at the same S/N. Top right shows artifacts introduced by poor phase sampling, in this case 10 bins even at high signal to noise (50). Bottom right panel is finally the case of insufficient resolution ( $150 \text{ km s}^{-1}$ ) to reconstruct the disc structure.

pattern is stable in the co-rotating frame, though its properties will change as the outburst progresses and especially when the cooling wave starts to turn the disc into quiescence again. Such time dependent behaviour can be tested by Doppler mapping of the disc as the outburst progresses. Godon, Livio & Lubow (1998) presented 2-D disc simulations using Fourier–Chebyshev spectral methods. They attempt to reproduce the observations of IP Pegasi. They find, however, that the spiral pattern resembles the observations only for very high temperatures. Unfortunately their  $\alpha$  values were rather low ( $\alpha = 0.1$  at most) and thus viscous spreading was less efficient compared to our simulations. As a consequence their discs were smaller by up to  $\sim 50\%$  compared to our model II simulation. Indeed, our model I simulation shows that in the case of low  $\alpha$  values little evidence of spiral arms in the emission lines is expected. However, with efficient viscous spreading the disc becomes large enough to result in a spiral pattern comparable to observed Doppler tomograms.

The behaviour of the emission lines in the presence of strong spiral waves is very different from axisymmetric or elliptically distorted accretion discs without spiral shock waves. In axisymmetric discs we expect a constant separation between the peaks, and in elliptical discs a smooth, sinu-

soidal variation with orbital phase, however without sudden jumps in the peak separation or the presence of multiple peaks arising from successive spiral arms such as in Fig. 4. Even though spiral arms in close binary accretion discs have been predicted more than 10 years ago (Sawada et al. 1986), and Doppler tomography provides a way of resolving the dynamics of accretion discs, a clear detection of a spiral pattern was only achieved in a recent outburst of IP Pegasi. Although confirmed since in this particular object (Harlaftis et al. 1999), detection of such a pattern in other systems is crucial.

We showed, however, that in small, cool discs, the observational signatures left by tightly wound spiral waves are small. Indeed, as Figure 6 shows, such discs, will closely resemble axisymmetric discs. The data on IP Pegasi and our simulations suggest that the increase in disc size and temperature during dwarf novae outbursts results in a prominent spiral pattern in the disc that can be recovered using tomography. The number of Doppler images of dwarf novae in outburst is unfortunately small. Marsh & Horne (1990) provide Doppler images of IP Pegasi in both quiescence and outburst. In particular their outburst map of HeII ( $\lambda 4686$ ) four days into outburst show a two armed enhancement in the disc at the correct positions in the tomogram. Their res-

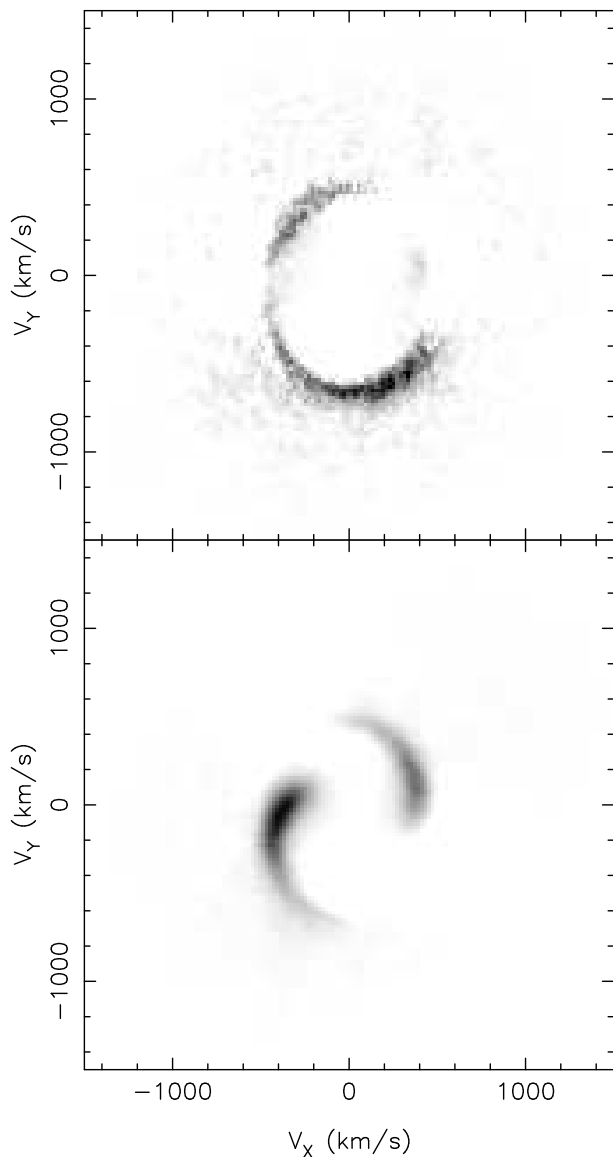


**Figure 8.** The asymmetric parts of the reconstructed images for the two models. In the high  $M$  case, only a slight asymmetry is produced in the top left and lower right regions. In the low  $M$  case, the image is dominated by the two armed spiral structure.

olution was unfortunately rather low ( $\sim 130 \text{ km s}^{-1}$ ). Piche & Szkody (1989) note that their outburst data of IP Peg is not compatible with a symmetric Keplerian disc, but no disc image is available. Similarly, Hessman (1989) reports measurements of the emission line peak velocities of IP Pegasi at the end of an outburst which shows a phase dependence that suggests a strong asymmetry in the outer disc persists well into the outburst, though is much weaker than in the initial phases. Outburst tomograms of SS Cyg (Steehgs et al. 1996) show a highly non-axisymmetric disc, again with enhanced emission in the top right and lower left areas. On the other hand, tomography of the disc in OY Car in outburst (Harlaftis & Marsh 1996) shows some evidence for the gas stream and its impact on the disc, but no clear spiral disc structure. Whether this is related to the fact that OY Car is a SU UMa type dwarf nova, will be explored in the future.

Nova-like variables provide permanent high mass transfer accretion discs, and we would therefore expect tidal structures to be important. Unfortunately the emission lines from these systems are poorly understood. The lines are single peaked and contain S-wave components of unknown origin. The exception could be V347 Pup, the only eclipsing nova-like variable with clear double peaked emission line profiles originating in the disc (Still et al. 1998, Steeghs et al., in preparation). The disc appears to be tidally distorted, and more data may confirm the presence of spiral structure in this system.

Conclusive remarks on the presence of spiral waves in accretion discs are therefore difficult to make with the sparse amount of outburst data available at this time. We have discussed the properties of CV discs since these are still the best laboratories to study the properties of thin,  $\alpha$  type accretion discs where most heating is due to viscous dissipation. In particular, high quality spectroscopic studies of dwarf novae throughout their outburst cycles are invaluable in understanding the physics of thin accretion discs. It is important to confirm with further observations that the spiral density distribution in close binary accretion discs is a common phenomenon and during which source states they can be observed.

The significance of tidal waves in the discs of X-ray binaries (Blondin & Owen 1997, Owen & Blondin 1997, Lanzafame & Belvedere 1998) is also considerable, since the Mach numbers in these discs are much lower and the relevance of density waves to the total angular momentum budget of the disc is therefore greater compared to CVs. In due course this should be accessible to similar observational tests.

## 6 SUMMARY

We studied the emission line profiles of close binary accretion discs in cases where the disc pattern is dominated by prominent spiral shock arms excited by the tidal forces of the secondary star. As underlying disc models we used the grid of full hydrodynamic CV disc calculations of Stehle (1999). We model the emission lines using the theory of Horne (1995), including the effect of shear broadening for saturated lines. Doppler tomograms and trailing spectra were constructed and instrumental effects were included to assess the data quality required to reconstruct spiral structure in CV discs.

We found that for high Mach number discs ( $M = v_\phi/c_s \simeq 15 - 30$ ) the spiral shock arms are too tightly wound to leave significant fingerprints in the emission line structure of these small discs. As a result the peak separation of the double peaked emission line profile varies only by  $\sim 8\%$  with binary phase. We therefore do not expect to detect strong spiral arms in quiescent CV discs.

For low Mach number discs ( $M \simeq 5 - 20$ ), i.e. for CV accretion discs in outburst, the line emissivity is dominated by the spiral shock arms. The two armed spiral pattern is identified by the presence of converging peaks in the line profiles. This signature in the trailing spectrum is expected to be sufficiently prominent that a signal to noise of  $\sim 15$  per pixel, a wavelength resolution of  $\sim 80 \text{ km s}^{-1}$  and a time resolution of 50 spectra per binary orbit is sufficient to

verify the presence of spiral shock arms in binary accretion discs through Doppler tomography of strong emission lines.

Our simulations successfully reproduce the emission line properties of the disc structure observed in IP Pegasi. The detection of strong two armed spiral arms in outburst (Steeghs et al. 1997), but no clear disc structure in quiescence (Marsh & Horne 1990), is convincingly reproduced by tidal spiral waves in the accretion disc.

The prospect of a new way to probe the local physics of discs through the dynamics of these tidal spirals demands more observational efforts on the detailed properties of high-mass transfer accretion discs through indirect imaging.

## ACKNOWLEDGEMENTS

We thank K. Horne and A. King for many stimulating discussions and for improving the language of the manuscript. Tom Marsh is thanked for the use of his DOPPLER package. R.S acknowledges a PPARC Rolling Grant for Theoretical Astrophysics to the Astronomy Group at Leicester.

## REFERENCES

- Armitage, P.J., Murray, J.R., 1998, MNRAS, 297, L81  
 Billington, I., Marsh T.R., Dhillon V.S., 1996, MNRAS, 287, 673  
 Blondin, J.M., Owen, M.P., 1997 in *Accretion Phenomena and Related Outflows*, ASP Conference Series Volume 121, 361  
 Frank J., King A., Raine D., 1992 *Accretion Power in Astrophysics*, Cambridge Astrophysics Series 21, Cambridge University Press  
 Godon, P., Livio, M., Lubow, S., 1998, MNRAS 295, L11  
 Harlaftis, E.T., Marsh, T.R., 1996, A&A, 308, 97  
 Harlaftis, E.T., Steeghs, D., Horne, K., Martin, E., Magazzu, A., 1999 MNRAS, in press  
 Heemskerk, M., 1994, A&A 288, 807  
 Hessman, F.V., 1989, AJ 98, 675  
 Horne, K., 1985, MNRAS 213, 129  
 Horne, K., Marsh, T.R., 1986, MNRAS 218, 761  
 Horne, K., 1995, A&A 297, 273  
 Lanzafame, G., Belvedere, G., 1998, MNRAS 295, 618  
 Larwood, J., 1997, PhD thesis, Queen Mary and Westfield College, London  
 Marsh, T.R., Horne, K., 1988, MNRAS 235, 269  
 Marsh, T.R., Horne, K., 1990, ApJ 349, 593  
 Owen, M.P., Blondin, J.M., 1997 in *Accretion Phenomena and Related Outflows*, ASP Conference Series Volume 121, 779  
 Paczyński, B., 1977, ApJ 216, 822  
 Piché F., Szkody P., 1989, AJ, 98(6), 2225  
 Robinson E.L., Marsh T.R., Smak J.I., 1993, in *Accretion discs in compact stellar systems*, ed. J.C.Wheeler, World Scientific  
 Różyczka, M., Spruit, H.C., 1989, in *Theory of Accretion Disks*, ed. F.Meyer et al. (Dordrecht, Kluwer), 351  
 Różyczka, M., Spruit, H.C., 1993, ApJ 417, 677  
 Savonije, G.J., Papaloizou, J.C.B., Lin, D.N.C., 1994 MNRAS 268, 13  
 Sawada, K., Matsuda, T., Hachisu, I., 1986, MNRAS 219, 75  
 Shakura, N.I., Sunyaev, R.A., 1973, A&A 24, 337  
 Smak, J., 1981, Acta Astr. 31, 395  
 Spruit, H., 1987, A&A, 184, 173  
 Spruit, H., Matsuda, T., Inoue, M., & Sawada, K., 1987, MNRAS 229, 517  
 Steeghs, D., Horne, K., Marsh, T.R., Donati, J.F., 1996, MNRAS, 281, 626  
 Steeghs, D., Harlaftis, E.T., Horne, K. 1997, MNRAS, 290, L28  
 Stehle, R., 1999, MNRAS, in press  
 Stehle, R., Spruit, H.C. 1999, MNRAS, in press  
 Still M.D., Buckley D.A.H., Garlick M.A., 1998, MNRAS, 299, 545  
 Warner, B., 1995, *Cataclysmic Variable Stars*, Cambridge Astrophysics Series 28, Cambridge University Press  
 Yukawa, H., Boffin, H.M., Matsuda, T., 1997, MNRAS, 292, 321